EFFECTS OF REVERBERATION AND NOISE ON THE ESTIMATION OF SYNTHETIC APERTURE SONAR MULTI-LOOK COHERENCE

AP Lyons University of New Hampshire, Center for Coastal and Ocean Mapping, Durham, New Hampshire, USA

JL King Naval Surface Warfare Center, Panama City, Florida, USA

DC Brown The Pennsylvania State University, Applied Research Laboratory, State College, Pennsylvania, USA

1 INTRODUCTION

First developed for ship detection with synthetic aperture radar[1, 2], multi-look coherence explores the phase information contained in synthetic aperture sonar (SAS) data by first splitting along-track and cross-track spatial bandwidth contained in a complex image into sub-bands and then estimating the coherence between the lower-resolution images formed from these sub-bands. In the presence of a random distribution of surface or volume scatterers, the spectral coherence is proportional to the degree of overlap in sub-bands of the SAS image. Consequently, for a perfectly random distribution of scatterers, the spectral coherence should be zero when the sub-bands do not overlap. If the scatterer distribution deviates from this basic random distribution, the coherence may be non-zero for special cases that would be related to scattering from specific structures such as points or facets. Based on preliminary experimental results, it appears to be possible to separate man-made targets from interfering background reverberation and clutter using coherence, as targets have features that scatter coherently in angle versus the random seafloor interface or volume which scatters incoherently. Characteristics of a target object may also be inferred as sub-band coherence is a sensitive function of both angle and frequency.

For multi-look coherence-based detection or classification, the key parameter is the magnitude of the complex correlation coefficient, γ. For two complex images this parameter is an estimate of the coherence between scenes. Typically the expectation operation used in estimating the correlation coefficient is evaluated using a spatial average, which lowers the spatial resolution of the resulting coherence map. The resolution of the coherence image will be a function of the original image resolution, the number of sub-look images formed from the original image and the number of samples used in the expectation. Reducing the size of the expectation window will increase spatial resolution but at the cost of increasing the bias and variance of the estimate. Increasing the expectation window size will reduce the bias and variance of the estimate but at the cost of introducing more background reverberation, reducing the overall value of coherence caused by a target in the window. It is also possible to form an additional expectation by combining estimates of $|\gamma|$over a number sub-look pairs of the scene in angle or frequency. When averaging independent coherence estimates from sub-look pairs, the resolution of the resulting average coherence image is equal to the spatial resolution of the coherence maps of the individual sub-looks while its variance is inversely proportional to the number of sub-looks. The advantages of averaging the coherence of sub-look pairs for variance reduction must be weighed, however, against the reduction in the number of coherence samples that will be available for target classification using the angular or frequency dependence of coherence.

In the sections that follow, we review and apply the relevant coherence estimation theory to explore the effects of target signal-to-noise ratio (SNR) and the number of samples used in forming the coherence map on the resulting coherence signal to background ratio (SBR). Example model-data comparisons will be shown for data collected off the coast of Florida by the Applied Physics Laboratory, University of Washington, using a rail-based SAS system during the 2004 Sediment Acoustics Experiment (SAX04)[3, 4].

2 ESTIMATION OF THE SIGNAL TO BACKGROUND RATIO IN THE COHERENCE IMAGE

The complex coherence for a pair of zero-mean complex signals x_1 and x_2 is defined by Born and Wolf[3] for stationary processes as the zero-lag correlation coefficient:

$$\gamma = \langle x_1 x_2^* \rangle / \sqrt{\langle |x_1|^2 \rangle \langle |x_2|^2 \rangle} \quad (1)$$

where $\langle \cdots \rangle$ represents the expectation operator. The coherence magnitude $|\gamma|$ is sometimes referred to as the "degree of coherence," or more often, simply "coherence". In practice, the sample coherence, $\hat{\gamma}$, is used as the coherence estimate, which implies ergodicity in x_1 and x_2. Given n measurements, the sample coherence is given by:

$$\hat{\gamma} = \sum_{i=1}^{n} x_1 x_2^* / \sqrt{\sum_{i=1}^{n} |x_{1i}|^2 \sum_{i=1}^{n} |x_{2i}|^2} \quad (2)$$

where i is the sample number. The sample coherence given by Equation (2) yields a coherence estimate which should be asymptotically unbiased as n increases[4]. In our application, n represents the values in a window centered on given complex image pixel for a pair of images. It is expected that the multilook coherence for targets will differ from that of natural background. To quantify this difference the signal-to-background ratio of coherence, SBR, is defined as

$$SBR = \frac{\langle |\gamma| \rangle'}{\langle |\gamma| \rangle} \quad (3)$$

where $\langle |\hat{\gamma}| \rangle'$ the multilook coherence estimated from a target region and $\langle |\hat{\gamma}| \rangle$ is the multilook coherence estimated from a non-target region.

Our interest is in the magnitude of the sample coherence, $|\hat{\gamma}|$, which is the maximum likelihood estimate of the coherence magnitude[5]. For a jointly complex-Gaussian process, an analytical expression for the probability density function of $|\hat{\gamma}|$ was derived by Touzi and Lopes[6] as a function of the coherence magnitude, $|\gamma|$, and the number of independent samples, n, used to form the sample estimate and is given by the expression:

$$p(|\hat{\gamma}|; |\gamma|, n) = 2(n-1)(1-|\gamma|^2)^n |\hat{\gamma}| (1-|\hat{\gamma}|^2)^{n-2} \, {}_2F_1(n, n, 1, |\gamma|^2 |\hat{\gamma}|^2) \quad (4)$$

where ${}_2F_1$ is the Gauss hypergeometric function, a special case of the generalized hypergeometric function, ${}_pF_q$. Equation (4) was used in Touzi and Lopes[6] to obtain an analytical expression for the first moment of $|\hat{\gamma}|$:

$$\langle |\hat{\gamma}| \rangle = \left(\frac{\Gamma(n)\Gamma(3/2)}{\Gamma(n+1/2)} \right) \cdot {}_3F_2 \left(\frac{3}{2}, n, n; n+\frac{1}{2}; 1; 0 \right). \quad (5)$$

Evaluation of Equation (5) shows that the sample coherence magnitude is biased towards higher values. This bias increases as the sample coherence magnitude approaches zero, with a maximum bias occurring at zero. In the application of multilook coherence for target detection, the increased levels of bias in the estimate for the non-target background, where no coherence is expected, will result in a reduction in the target signal-to-background ratio of coherence, SBR. The bias in the coherence estimate decreases with increasing number of independent samples, as the maximum-likelihood estimate is asymptotically unbiased.

If we assume that the signal-to-noise ratio (SNR) for a target is identical between two complex images that are being correlated, then the sample coherence estimate after the addition of incoherent noise becomes[7]:

$$\langle|\hat{\gamma}|\rangle' = \langle|\hat{\gamma}|\rangle \left(\frac{SNR}{1+SNR}\right) \quad (6)$$

This SNR term in Equation (6) can contain any sources of incoherent noise, including system noise, multipath interference, ambient noise or any non-target seafloor areas that are included in a pixel after multilook processing. This term is difficult to estimate in practice, but for this work, we will simply use the ratio of the average intensity of a target in a complex SAS image to the surrounding seafloor background level (which has a value of 1 in our case as we have normalized our data). We acknowledge that our approximation for the SNR here is suspect and may be the source of the modest model-data disagreement seen in comparisons shown in the next section.

Although increasing the number of samples used to form the sample coherence magnitude will improve the estimate for non-target background, increasing the estimation window size will also necessarily include samples of unwanted reverberation noise into the estimate of coherence for the target. This has the undesirable effect of reducing the coherence of the target and thereby decreasing the SBR. Reverberation from the sediment in a complex SAS image is assumed to behave like an incoherent source, adding noise to a coherent signal. Under some specific simplifying assumptions, the assumed incoherent scattering of the background reverberation leads to the practical statement that adjacent resolution cells are uncorrelated, i.e., independent. Under the reverberation model given above, we treat any uncorrelated background reverberation in our as sampling window as the addition of incoherent noise and simply scale our original target SNR by the additional non-target area included in the estimation window. This additional area is directly proportional to the number of samples, n, so that we can replace the SNR in Equation (6) by SNR/n. As the window size is increased, the effective SNR is reduced in our sample coherence estimate. It is important to note that decorrelation due to this addition of non-target background will always be present in multilook processing and is likely to be the dominant factor in the decreasing the coherence value in the absence of multipath.

For this study we want to understand the relative levels of target coherence to background coherence as we vary our estimation window size. Combining Equations (5) and (6) yields the coherence signal-to-background ratio, SBR, for multilook processing with no overlapping bands in along-track spatial wavenumber:

$$SBR = \frac{\langle|\gamma|\rangle\left[\frac{SNR}{n}/\left(1+\frac{SNR}{n}\right)\right]}{\left(\frac{\Gamma(n)\Gamma(3/2)}{\Gamma(n+1/2)}\right)\cdot {}_3F_2\left(\frac{3}{2},n,n;n+\frac{1}{2};1;0\right)} \quad (7)$$

Figure 1 shows the effects of increasing the estimation window size on the SBR estimate as a whole for a given target SNR of 16 dB (blue line). The numerator and denominator terms in the SBR of equation (7) are also shown separately by holding one constant while varying the other to highlight their individual effects on the overall SBR shape. For a low number of samples in the estimation window, the SBR is seen to have a low value caused by the large bias in the maximum-likelihood estimator. For a high number of samples, the SBR also has a low value, but now caused by the large number of non-target samples that have been included in the estimate. At intermediate values of sample number, the SBR has a maximum value, which will be the optimum window size for target detection. This maximum, or optimum window size, depends on the initial target SNR in the complex image. Figure 2 displays the SBR as a function of the initial target SNR and window size. It can be seen in this figure that the optimum window size moves to higher values as the target signal-to—noise ratio is increased. Higher target signal levels allow more background reverberation to be included in the estimate without decreasing the SBR. Equation (7) will be compared to experimental results of target signal coherence to background coherence in the following section.

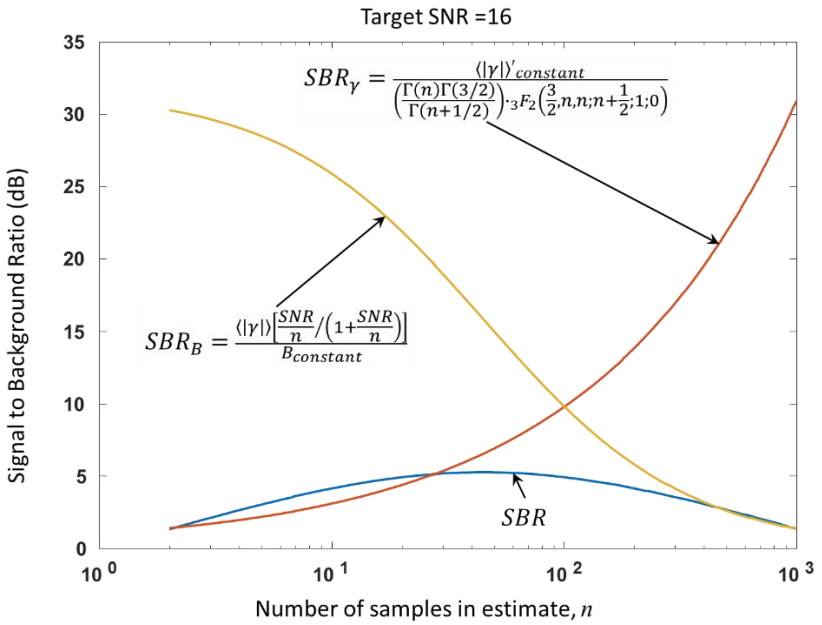

Figure 1: Target Signal to Background results from Equation (7) (blue line). The yellow and red lines show the numerator of Equation (7) holding the denominator constant and the denominator of Equation (7) holding the numerator constant, respectively. An optimum window size can be seen in the SBR due to the competing mechanisms of estimation bias and added background noise in the estimation window.

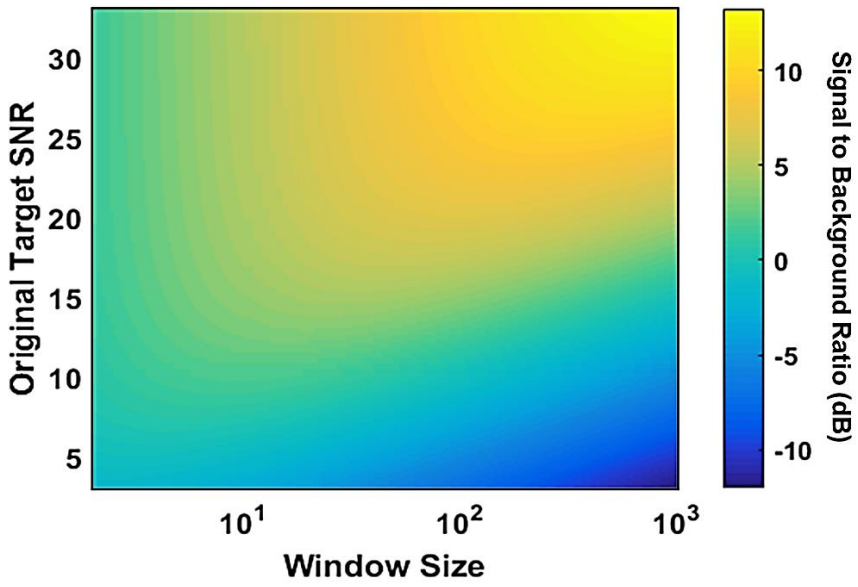

Figure 2: Signal-to-background results from equation (7) as a function of the target SNR and window size. The optimum window size is seen to shift to larger values as target SNR is increased.

3 APPLICATION TO SAS DATA

Having established the theoretical framework within which to interpret the effects of window-size on the signal-to-background ratio for coherence in multilook processing, we next investigate the applicability of these results by comparison to real data. The data used for our analysis was collected as part of the SAX04 experiment that took place on a rippled sandy seafloor off of Panama City, Florida in the fall of 2004. The acoustic system was operated by the Applied Physics Laboratory at the University of Washington and consisted of transmitters and receivers mounted on a tower which moved along a 28 m rail. A synthetic aperture was formed using returns from transmissions made along the length of the rail. We made use of data collected in two different frequency bands, 12 – 28 kHz with a 42 degree beamwidth, and 30 – 50 kHz with a 21 degree beamwidth. The top left image in Figure 3 displays an example of a 30 – 50 kHz SAS image taken during SAX04 with ripples and a large variety of clutter evident in the figure. In this figure, man-made targets are circled in green and included a buried sphere at 10 m range and 7 meters along track, a partially-buried cylinder at 30 m range and 22 m along track, two floats at 23 m range, 3 m along track and 37 m range and 6 m along track respectively, and an unknown target at 30 m range and 22 m along track. In addition to strongly scattering patches, ripples, and fish schools, target-like clutter appears at 30 m range 1 m along track and 37 m range and 10 m along track and are circled in red on Figure 3.

The processing chain for the results presented below consisted in taking complex SAS images, such as those used to form the example intensity image shown in Figure 3, and transforming them into the wavenumber domain. The full band is then filtered into non-overlapping sub-bands (or 'looks') in along-track wavenumber. The sub-bands are then transformed back into the spatial domain as complex images with lower resolution. The complex cross-correlation can then be estimated between these images with different looks in angle and coherence examined as a function of target and window size. The top right and bottom left and right images in Figure 3 show coherence maps for the broadside pair of looks (out of 6 sub-looks) formed using the same 30 – 50-kHz band complex image used for intensity image in Figure 3. The three coherence maps use different estimation window sizes.

For the coherence map formed using the largest two estimation window sizes, the man-made targets (circled in green in the intensity image in Figure 3) are clearly detected in the coherence map with correlation coefficient values above 0.8, while the seafloor background (ripples, patches with high scattering) and clutter objects (circled in red in the intensity image in Figure 3) display low levels of coherence. The reduction in background coherence bias is evident as a larger number of samples was used in estimating the coherence (as is the loss in resolution of the coherence map). The SBR is seen to increase with window size for all man-made targets seen for this data set. Another tradeoff to consider when increasing estimation window size to increase SBR is the loss in spatial resolution of the final coherence map.

As described in the previous section, for a random distribution of scatterers when the wavenumber bands used in forming sub-band images do not overlap, the estimated coherence for the background should have a minimum value which depends on the finite window size used to form the correlation coefficient. The target signal coherence estimate will depend on additional non-target reverberation included in the estimation window. Figure 4 shows results of coherence signal-to-background estimated for SAS data from both the 12 – 28 kHz band and the 30 – 50 kHz band. Predictions based on Equation (7) are also shown as solid lines on this figure for initial target SNRs of 15, 20 and 25 dB. Comparisons for the 12 – 28 kHz data are quite good, with the shift in optimal number of samples with increasing SNR captured well. The 30 – 50 kHz dataset shows less agreement, but is still satisfactory. Discrepancy could be due to a variety of factors, including mis-estimation of the original target signal-to-noise ratio or frequency/aspect dependent scattering effects for specific targets.

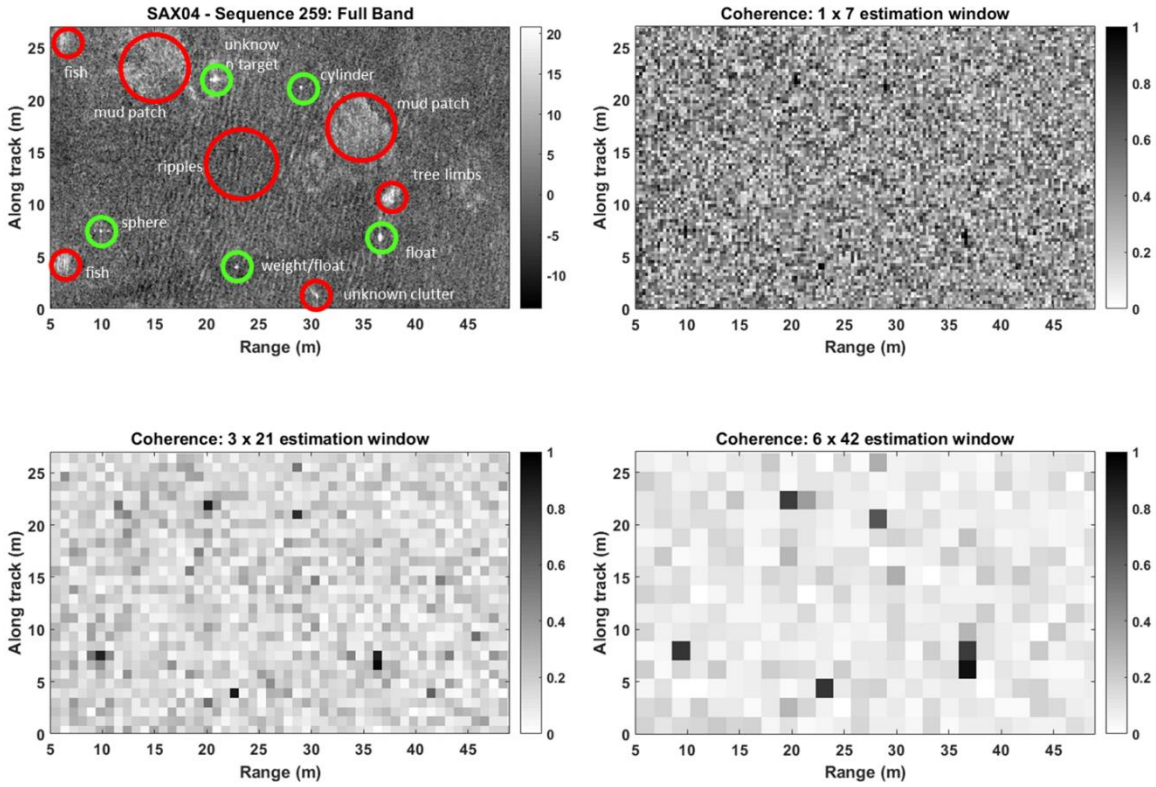

Figure 3: 30-50 kHz SAX04 rail-SAS intensity image (top left) includes buried, partially buried and proud targets on rippled sand (circled in green) and clutter objects (circled in red). Coherence estimated between a pair of sub-band images formed from the same 30 – 50 kHz dataset for variously-sized coherence estimation windows. $\mathcal{SBR}$ increases as estimation bias for the background decreases with larger window sizes.

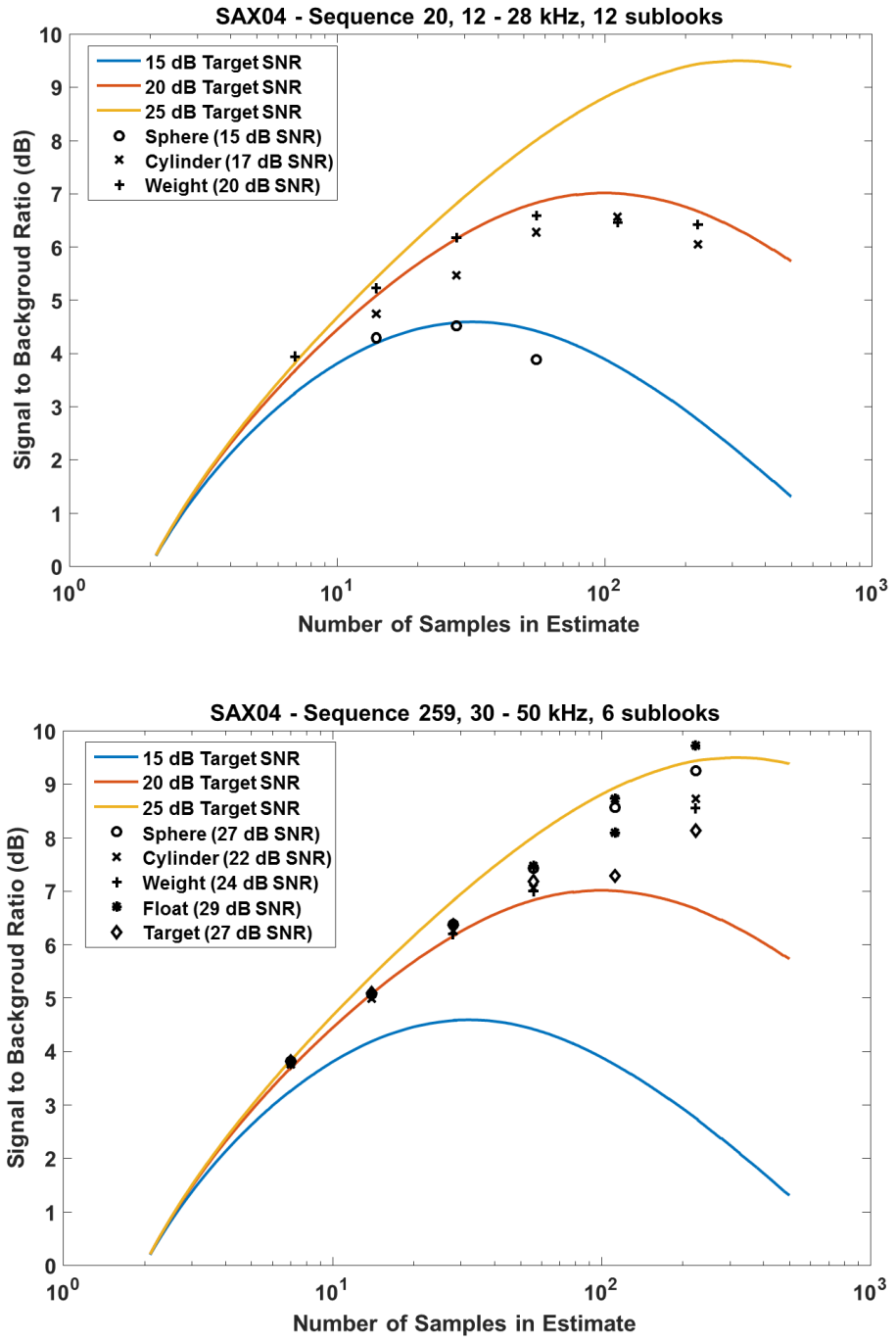

Figure 4: Estimates of coherence signal to background for targets found in sequences 20 (top) and 259 (bottom) from the SAX04 SAS data set described in the text. In these plots, the solid lines are predictions made using Equation (7) for various levels of target on background signal to noise ratio. Symbols on these plots are results for individual targets with their SNR given in the legend.

4 SUMMARY

In this paper, we have presented predictions of the impact of estimation window size on target signal-to-background ratio, SBR, for coherence maps produced as part of multilook SAS processing for target detection. This was accomplished by including both the inherent bias of the maximum-likelihood estimator for coherence and the coherence degradation caused by inclusion of non-target background reverberation into the estimate into an estimate for SBR. For the two experimental datasets considered here, SBR increased or showed an optimal window size in agreement with predictions. Increasing estimation window size to increase SBR results in loss of spatial resolution in the final coherence map, which may be a consideration in choosing a window size for target detection using the multilook coherence technique. Knowledge gained as part of this study will help to determine the performance of multilook technique for target detection.

5 ACKNOWLEDGMENTS

The authors would like to thank Kevin Williams and Steve Kargl of the Applied Physics Laboratory, University of Washington, Seattle, for supplying the SAX04 experimental SAS data shown in this paper and for providing ancillary data. For the work presented in this paper, APL was supported under ONR Grant N00014-16-1-2469.

6 REFERENCES

1. Arnaud, A. (1999) Ship detection by SAR interferometry. In *Proceedings of the IEEE 1999 International Geoscience and Remote Sensing Symposium*, Hamburg, Germany, 28 June–2 July 1999; Volume 5, pp. 2616–2618.
2. Ouchi, K., Tamaki, S., Yaguchi, H., & Iehara, M. (2004) Ship detection based on coherence images derived from cross correlation of multilook SAR images. *IEEE Geosci. Remote Sens. Lett*., 1,184–187.
3. Thorsos, E. I., Richardson, M. D., & Lynch, J. F. (2009). Special issue on sediment acoustic processes (Part II) - Guest Editorial. *IEEE Journal of Oceanic Engineering*, *34*(4), 369.
4. Williams, K. L., Jackson, D. R., Tang, D., Briggs, K. B., & Thorsos, E. I. (2009). Acoustic backscattering from a sand and a sand/mud environment: Experiments and data/model comparisons. *IEEE Journal of Oceanic engineering*, *34*(4), 388.
5. Born, M., & Wolf, E. (2013). *Principles of optics: electromagnetic theory of propagation, interference and diffraction of light*. Elsevier.
6. Touzi, R., Lopes, A., Bruniquel, J., & Vachon, P. W. (1999). Coherence estimation for SAR imagery. *IEEE Transactions on Geoscience and Remote Sensing*, *37*(1), 135-149.
7. Touzi, R., & Lopes, A. (1996). Statistics of the Stokes parameters and of the complex coherence parameters in one-look and multilook speckle fields. *IEEE Transactions on Geoscience and Remote Sensing*, *34*(2), 519-531.
8. Brown, D. C. (2017). “Modeling and measurement of spatial coherence for normal incidence seafloor scattering,” Ph.D. thesis, The Pennsylvania State University.